Applied Catalysis B: Environmental 140–141 (2013) 537–545

Contents lists available at SciVerse ScienceDirect

Applied Catalysis B: Environmental

journal homepage: www.elsevier.com/locate/apcatb

# Transition metal coated $TiO_2$ nanoparticles: Synthesis, characterization and their photocatalytic activity

Gulin Selda Pozan*, Meltem Isleyen, Sinem Gokcen

*Istanbul University, Faculty of Engineering, Chemical Engineering Department, Avcilar, 34320 Istanbul, Turkey*

ARTICLE INFO

*Article history:*
Received 28 December 2012
Received in revised form 15 April 2013
Accepted 17 April 2013
Available online 26 April 2013

*Keywords:*
Photocatalytic degradation
Phenol
Transition metal oxide
$TiO_2$
UV irradiation
Characterization

ABSTRACT

Transition metal ions (M–$TiO_2$, where M = Cu(II), Ni(II), Co(II) and Fe(III)) loaded $TiO_2$ catalyst were successfully prepared by solid-state dispersion method. The catalysts were characterized by X-ray diffraction (XRD), X-ray photoelectron spectroscopy (XPS), Fourier transform infrared spectroscopy (FT-IR), diffuse reflectance spectroscopy (DRS), transmission electron microscopy (TEM), Brunauer–Emmett–Teller (BET). Photocatalytic activities of bare and CuO, NiO, $Co_3O_4$, $Fe_2O_3$ loaded $TiO_2$ catalysts were compared and the rate constant values were determined from the kinetic studies of the degradation of phenol. The extent of degradation of phenol and its mineralization were confirmed further by HPLC and TOC analyses. The 0.1CuO wt% $TiO_2$ showed the highest percentage of phenol degradation (100%) and highest reaction rate (0.99 mg $l^{-1}$ $min^{-1}$) in 90 min. It was also found that the catalytic activity of 0.1CuO–$TiO_2$ was found to be higher than nano $TiO_2$ and P-25 photocatalyst. The profound effect of transition metal oxide catalyst for phenol degradation is generally considered due to the high surface area, small particle size, and high dispersion of CuO, and the presence of more surface OH groups than that of the pure $TiO_2$ photocatalyst.



## 1. Introduction

Aqueous effluent streams originating from many industries contain organic pollutants and metal ions too law to make their recovery easy but too high to be discharged to the environment without prior treatment [1]. Phenol and its derivatives' degradation products in the environment are major aquatic pollutants. Since they are stable and soluble in water, their removal to reach safety levels in the range 0.1–1.0 mg/L is not easy [2]. Traditional methods such as solvent extraction, activated carbon adsorption, and common chemical oxidation often suffer from serious drawbacks including high cost or formation of hazardous by-products [3,4]. Biological degradation is environmental friendly and cost effective; but it is usually time-consuming [4]. Among the methods available, oxidative degradation using photocatalysts appears cost effective, which has thus been an increasingly important process in pollution prevention [5–7]. The advantages of photocatalysis include low operation temperature, low cost and significantly low energy consumption. These factors have led the relevant application of photocatalysis to the stage of commercialization.

Photocatalytic degradation of such organic pollutants with $TiO_2$ semiconductor has been proved to be more efficient and popular method because the titanium dioxide ($TiO_2$) is an effective photocatalyst owing to its high efficiency, low cost, inertness, strong oxidizing power, non toxicity and stability within a wide range of pH, and in expensive photosensitized material [8–10]. However, some disadvantages of $TiO_2$ for industrial applications are the need of filtration and its difficulty for sedimentation after photocatalytic process after the photodegradation process. High band gap energy (ca. 3.2 eV for anatase), low photo quantum efficiency, and high recombination of electron–hole pairs restricted the application of titania [11].

If $TiO_2$ was coupled with some transition metals to form the binary oxide, it is highly possible to achieve novel photocatalytic materials for effective removal of organic pollutants from the industrial wastes.

Recently, the research has been focused on modifying the surface or bulk of the semiconductor catalyst by adding transition metal impurities, which give rise to the mixed oxide semiconductors formation [12]. It has been reported that the addition of Pt [13], $Cr^{3+}$ [14], $Cu^{2+}$ [15], $Fe^{3+}$ [16–20], V, Ni, Co, Au, Pd or other cation into anatase titania can improve its photoactivity. Pd, Rh, Au are expensive transition metals. The band gap of titanium dioxide would be decreased and visible light absorption would be increased owing to the incorporation of some transition metals.

Some studies have shown that, preparation of titania nanoparticles with transition metals such as Fe, Co, and Ni dopants, showing a photocatalytic capability of organic dye under visible illumination [21]. In addition, the metal-containing titanium particles, plays

* Corresponding author. Tel.: +90 212 473 70 70x17789; mobile: +90 533 780 64 21.
*E-mail address:* gpozan@istanbul.edu.tr (G.S. Pozan).

0926-3373/$ – see front matter © 2013 Elsevier B.V. All rights reserved.
http://dx.doi.org/10.1016/j.apcatb.2013.04.040

a major role in the removal of a group of serious environmental pollutants such as phenols.

Several methods have used to synthesize Fe-loaded $TiO_2$ nanoparticles, such as sol–gel method [15], impregnation [22] and hydrothermal method [20]. However, above methods, have some disadvantages for industrial applications. For example, the sol–gel process is more common but needs high temperature (>500 °C) for obtaining $TiO_2$ crystalline particles. Hydrothermal method also requires long reaction time.

Although it has been reported that the solid-state dispersion (SSD) method has the advantage in preparation of catalyst, the modification of some transition metals with $TiO_2$ has not yet been reported.

In the present work, we examined the effect of added transition metal oxides on the efficiency of photocatalytic oxidation of phenol in aqueous solution. To achieve this goal, we have combined the structural and surface effect of different doping methods used in the preparation procedure, and the presence of transition metal oxides (CuO, NiO, $Co_3O_4$, $Fe_2O_3$) loading. The structural characteristics, morphology, percentage of concentrations were achieved by employing X-ray diffraction (XRD), diffuse reflectance spectroscopy (DRS), transmission electron microscopy (TEM), Brunauer–Emmett–Teller (BET) analysis of surface area.

## 2. Experimental

### 2.1. Materials

Starting materials for catalyst preparation were $Cu(NO_3)_2{\cdot}3H_2O$, $Ni(NO_3)_2{\cdot}6H_2O$, $Co(NO_3)_2{\cdot}6H_2O$, $Fe(NO_3)_3{\cdot}9H_2O$ (reagent grade, Aldrich), ammonia solution (25% in water), ethanol (absolute), titanium tetrachloride (≥99%) and P25 (consisting of 75% anatase and 25% rutile with a specific BET-surface area of 50 $m^2\,g^{-1}$ and primary particle size of 20 nm). The organic compounds used in the photocatalytic experiments were phenol, hydroquinone, catechol, and methanol (for HPLC, ≥99%) and were purchased from the Fluka Company and used without further purification. Deionized (D.I.) water was used for the preparation of all the catalysts as well as to dilute the phenol solution.

### 2.2. Catalyst preparation

$TiO_2$ nano-powders were prepared titanium tetrachloride and deionized water as the starting materials [23].

CuO, NiO, $Co_3O_4$, $Fe_2O_3$ were prepared by co-precipitation. An appropriate amount of metal nitrate ($Cu(NO_3)_2{\cdot}3H_2O$, $Ni(NO_3)_2{\cdot}6H_2O$, $Co(NO_3)_2{\cdot}6H_2O$, $Fe(NO_3)_3{\cdot}9H_2O$) was dissolved in deionized hot water and the resulting solution was heated up to 65 °C. This mixture was precipitated by gradually adding $NH_3$ solution (25 wt%) until pH value reached at 10. The resultant solution was slowly stirred for 2 h at 65 °C. After that, solution was irradiated under 500 W microwave for 3 min. The precipitate was then filtered, washed with deionized water and dried at 100 °C for 20 h and calcined at 500 °C for 5 h.

### 2.3. Synthesis of Cu, Ni Fe and Co loaded-$TiO_2$

The metal oxides catalysts were prepared by solid-state dispersion (SSD) method. SSD initially involves mixing of metal oxide and $TiO_2$ thoroughly using ethanol in agate mortar, the solvent was then removed by evaporation while mixing. Samples prepared by this method were dried at 110 °C and calcined at 450 °C for 6 h to obtain binary oxide catalysts. The resultant binary oxide was ground at a constant vibration rate of 300 rpm for 15 min in a Retsch MM 200 vibrant-ball mill by 12 mm $ZrO_2$ milling ball in $ZrO_2$ milling container. MO loading of the catalysts was nominally 0.05, 0.1, and 0.5 wt% and reported as the weight percentage. For instance, 0.05CuO–$TiO_2$ means that the catalyst contained nominally 0.05% CuO by weight.

In addition, 0.1CuO/$TiO_2$ catalyst prepared by incipient wetness impregnation (IMP) method to compare the effect of preparation method on the photocatalytic degradation reaction.

Copper (II) nitrate solution was prepared by dissolving $Cu(NO_3)_2{\cdot}3H_2O$ in distilled water. $TiO_2$ crystallites homogeneously were added in ceramic dish. Then, the precursor solution was slowly dropwised in the pure $TiO_2$ crystallites to obtain a paste. The obtained paste was dried and this process was continued until solution is complete. The impregnated $TiO_2$ was dried at 105 °C for 16 h, and it was calcined in air at 500 °C for 3 h. The resultant CuO loaded $TiO_2$ was ground at a constant vibration rate of 300 rpm for 15 min in a Retsch MM 200 vibrant-ball mill by 12 mm $ZrO_2$ milling ball in $ZrO_2$ milling container.

### 2.4. Catalyst characterization

The composition of the catalyst was determined using Thermo Elemental X Series ICP-MS.

Powder X-ray diffractions of samples were obtained using a Rigaku D/Max-2200 diffractometer with the CuKα (λ = 1.540) radiation. Samples were scanned from 10 to 80 at a rate of 2 °/min (in $2\theta$). The sizes of the crystalline domains were calculated by using the Scherer equation, $t = C\lambda/B\cos\theta$, where λ is the X-ray wavelength (Å), $B$ is the full width at half maximum, $\theta$ is Bragg angle, $C$ is a factor depending on crystallite shape (taken to be one), and t is the crystallite size (Å).

The surface OH groups of the photocatalyts were determined by FTIR spectroscopy using KBr in the form of pellets (Perkin Elmer Precisely Spectrum One).

The BET surface areas of the samples were determined by nitrogen adsorption–desorption isotherm measurement at 77 K (Quantachrome Inst.). The samples were degassed at 200 °C prior to the actual measurements.

The morphology and size distribution of the photocatalysts were recorded by scanning electron microscopy (JEOL/JSM-6335F) and transmission electron microscopy (JEOL HRTEM 2100). Diffuse reflectance spectra were obtained using a Schimadzu-3600 (UV–vis–NIR). $BaSO_4$ was used as the reflectance standard in the experiments.

The X-ray photoelectron spectroscopy (XPS) was performed on the SPECS EA 300 with an Al monochromatic anode.

### 2.5. Evaluation of photocatalytic activity

The photoactivity studies were carried out at atmospheric pressure and room temperature (298 K). In a typical experiment, 100 mg catalyst was dispersed in 50 mL phenol solution of initial concentration 25 mg/L and neutral pH (pH = 5) under magnetic stirring.

Phenol photooxidation runs were done with quartz batch-photoreactor of cylindrical shape. LUZCHEM LZC-5 photoreactor system was used in all experiments. The light source used was 64 W UV-B lamp (LUZCHEM LZC-UVB). UV-B lamp has maximum light intensity at 312 nm and the illumination distance is 18 cm from the target. The light intensity of UV lamp used for degradation experiments was recorded with an UV/vis powermeter (Smart Sensor-AR823). The photoreactor system had a magnetic stirrer and it was used to achieve uniform conditions in the reacting mixture. Before the UV light was turned on, the solution was stirred for 60 min to ensure good adsorption equilibrium between the catalyst and the solution. After irradiation for 5 h, the phenol solution was filtered through a membrane filter (pore size 0.45 mm) and the filtrate was used for TOC measurement with a TOC-V, Shimadzu equipment. The concentration of phenol and products were

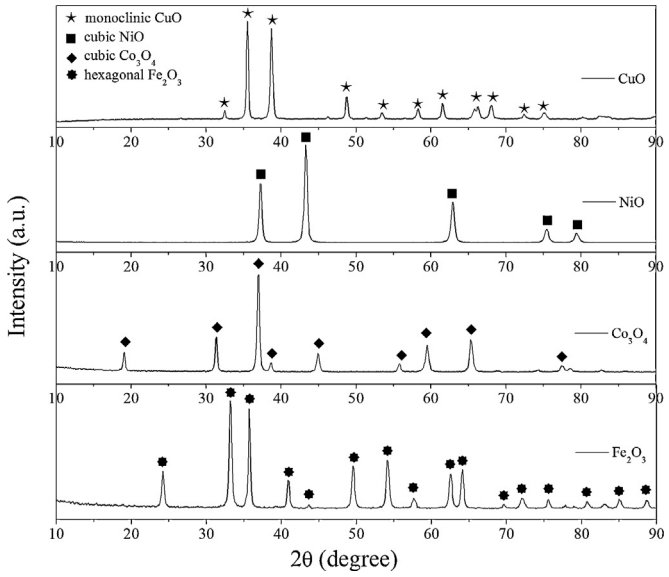


**Fig. 1.** XRD patterns of metal oxides (CuO, NiO, $Co_3O_4$ and $Fe_2O_3$).

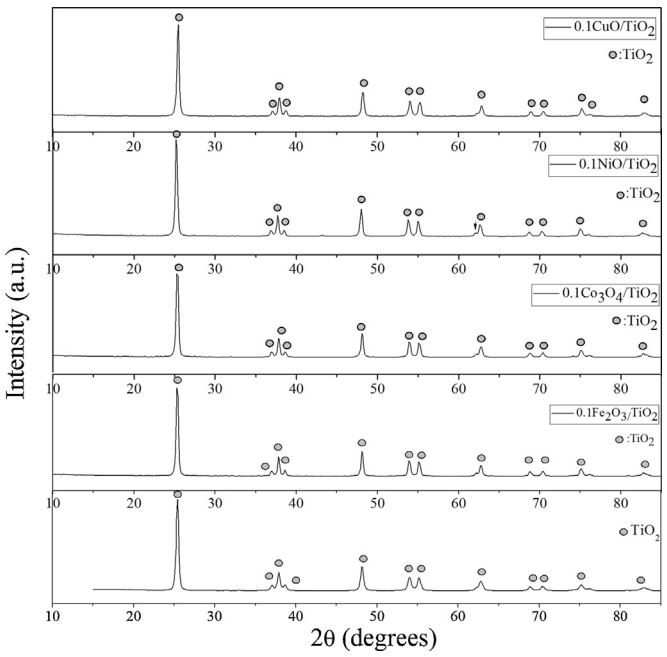


**Fig. 2.** XRD patterns for bare $TiO_2$, CuO(0.05%, 0.1% and 0.5%)/$TiO_2$, NiO(0.1%)/$TiO_2$, $Fe_2O_3$(0.1%)/$TiO_2$ and $Co_3O_4$(0.1%)/$TiO_2$ catalysts.

analyzed by HPLC (Thermo Scientific-TSP Model) equipped with C-18 column. The mobile phase used in HPLC was a mixed solvent of methanol and water (60/40, v/v) with a flow rate of 1 ml/min.

## 3. Results and discussion

### 3.1. Catalyst characterization

The actual weight percentages of the catalysts in the binary oxide catalysts were obtained by ICP-MS analysis. The calculated wt% of the catalysts and the ICP-MS values were almost similar. Furthermore, ICP-MS values of the catalysts clearly suggest that there may not be any noticeable differences between the calculated values and ICP values.

#### 3.1.1. BET surface area

The specific surface areas of catalysts were measured and the values are listed in Table 1. When the surface area values of bare titania and metal oxide loaded titania were compared, bare titania was found to have higher surface area than metal oxide loaded catalyst (except 0.1CuO/$TiO_2$). This is due to the increasing coverage of surface by the metal ions, which prevents the entry of nitrogen probe molecule. The large decrease in surface area was observed for 0.1 wt% $Fe_2O_3$ loaded titania catalysts when compared to 0.1 wt% CuO loaded titania catalysts. This suggests that finer $Fe_2O_3$ particles would have been formed on the surface of titania nano particles.

#### 3.1.2. X-ray diffraction analysis

Fig. 1 shows the XRD patterns of metal oxides (CuO, NiO, $Co_3O_4$, $Fe_2O_3$). The diffraction patterns of bare $TiO_2$, CuO(0.05%, 0.1% and 0.5%)/$TiO_2$, NiO(0.1%)/$TiO_2$, $Fe_2O_3$(0.1%)/$TiO_2$ and $Co_3O_4$(0.1%)/$TiO_2$ catalysts are depicted in Fig. 2. All the peaks were identified; indexed using the data available from the Joint Committee for Powder Diffraction studies (JCPDS) and the corresponding planes were indicated in Figs. 1 and 2.

XRD patterns indicate high crystallinity for all the catalysts. Anatase $TiO_2$, monoclinic CuO (JCPDS-05-0661), cubic NiO (JCPDS-78-0643), cubic $Co_3O_4$ (JCPDS-78-0643) and hexagonal $Fe_2O_3$ (JCPDS-33-0664) were the major crystalline phases detected on the X-ray diffraction patterns. Peaks appearing at 2$\theta$: 25.4, 37.0 37.9, 38.6, 47.9, 54.0, 55.2, 62.9, 68.9, 70.4, 75.2, 76.2, 83.1 correspond to the diffraction patterns of (1 0 1), (1 0 3), (0 0 4), (1 1 2), (0 0 0), (1 0 5), (2 1 1), (2 0 4), (1 1 6), (2 2 0), (2 1 5), (3 0 1) and (2 2 4), respectively, of the pure anatase phase of $TiO_2$. The reflections at 2$\theta$ = 25.3°, 48.2° and 37.8° confirmed the presence of anatase phase (JCPDS No. 89-4921), the absence of peak at 27.4° and 30.8° confirm that both rutile and brookite phases were absent [24]. No observable peaks were obtained for the impregnation of metal oxide (CuO, NiO, $Co_3O_4$ and $Fe_2O_3$) over $TiO_2$. This may be due to the less amount of loading of metal oxide over titania [25].

The crystallite sizes of the catalysts are calculated according to the Scherrer Formula and the results are listed in Table 1. $TiO_2$ crystallite size increased as copper oxide content increased.

#### 3.1.3. UV diffuse reflectance spectroscopy

Band gap measurements from diffuse reflectance studies will pave way to understand the optical response of the catalysts. The DRS spectra was taken for bare ($TiO_2$) and transition metal oxide loaded titania catalysts and shown in Fig. 3.

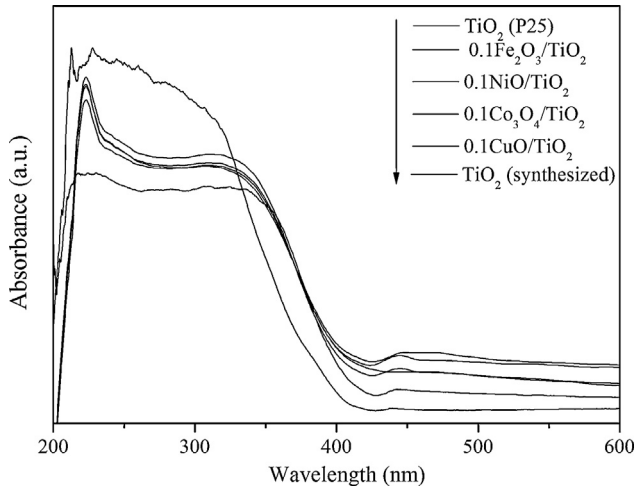


**Fig. 3.** UV–vis diffuse reflectance spectra of catalysts.

**Table 1**
The crystallite sizes, specific surface areas, band gap, crystal structure of materials and phenol degradation efficiencies over 90 min (%).

| Catalyst | Crystallite size (nm) | $S_{BET}$($m^2\ g^{-1}$) | Band gap (eV) | Crystal structure | $k_r$[a] | Phenol degradation efficiencies over 90 min (%) |
|---|---|---|---|---|---|---|
| 0.05 $CuO/TiO_2$ | 28 | 38 | 2.72 | Monoclinic | 0.36 | 80 |
| 0.1 $CuO/TiO_2$ (SSD) | 32 | 41 | 2.64 | Monoclinic | 0.99 | 100 |
| 0.1$CuO/TiO_2$ (IMP) | 41 | 32 | 2.75 | Monoclinic | 0.23 | 68 |
| 0.5 $CuO/TiO_2$ | 38 | 28 | 2.32 | Monoclinic | 0.25 | 40 |
| 0.1 $Fe_2O_3/TiO_2$ | 51 | 30 | 2.72 | Hexagonal | 0.19 | 68 |
| 0.1 $Co_3O_4/TiO_2$ | 45 | 35 | 2.69 | Cubic | 0.45 | 85 |
| 0.1 $NiO/TiO_2$ | 38 | 36 | 2.67 | Cubic | 0.81 | 87 |
| $TiO_2$ (synthesized) | 43 | 40 | 3.09 | Anatase | 0.55 | 88 |
| $TiO_2$-Degussa P25 | 32 | 50 | 3.12 | 70% Anatase + 30% rutile | 0.62 | 90 |

[a] Reaction rate constant (mg/Ldk).

From the DRS spectra the band gap values for all the catalysts were calculated using the formula $E_g = 1240/\lambda$ and given in Table 1, where $\lambda$ is the cut-off wavelength. Among all the synthesized catalysts, bare titania showed the maximum band gap value of 3.1 eV. The shifting of optical response of loaded catalysts to visible region can well be understood from the decrease in the band gap value from 3.1 eV. Large decrease in the band gap value was observed for CuO loaded titania catalysts than $Fe_2O_3$ loaded titania catalysts.

### 3.1.4. Transmission electron microscopy (TEM)

TEM images of bare titania and transition metal oxide impregnated titania catalysts are shown in Fig. 4(a)–(d). TEM images indicated that the titania particles are agglomerated and have different shapes and sizes. The average particle size of pure $TiO_2$ is around 65 nm in irregular sizes. 0.1$CuO/TiO_2$ catalyst has uniform morphology with the particle size of 30–40 nm, whereas, 0.1$NiO/TiO_2$, 0.1$Co_3O_4/TiO_2$ and 0.1$Fe_2O_3/TiO_2$ are in irregular sizes and shapes and also the particle size of 0.1$NiO/TiO_2$ 0.1$Co_3O_4/TiO_2$ and $Fe_2O_3/TiO_2$ are around 25–60 nm, 15–60 nm, 20–80 nm, respectively. These results are in good agreement with XRD data. TEM pictures and (Energy Dispersive Spectroscopy) EDS analyze of catalysts gave convincing evidence for the presence of metal oxide on the surface nano $TiO_2$. CuO dispersion was observed on the whole surface of nano $TiO_2$ in comparison to NiO, $Co_3O_4$ and $Fe_2O_3$. It has high photocatalytic activity because of the homogenously high dispersion on nano $TiO_2$. This study clearly established the role of $Cu^{2+}$ in decreasing the size of nano $TiO_2$.

The morphology of the catalyst prepared by impregnation method is different from SSD method. The primary particles exhibit

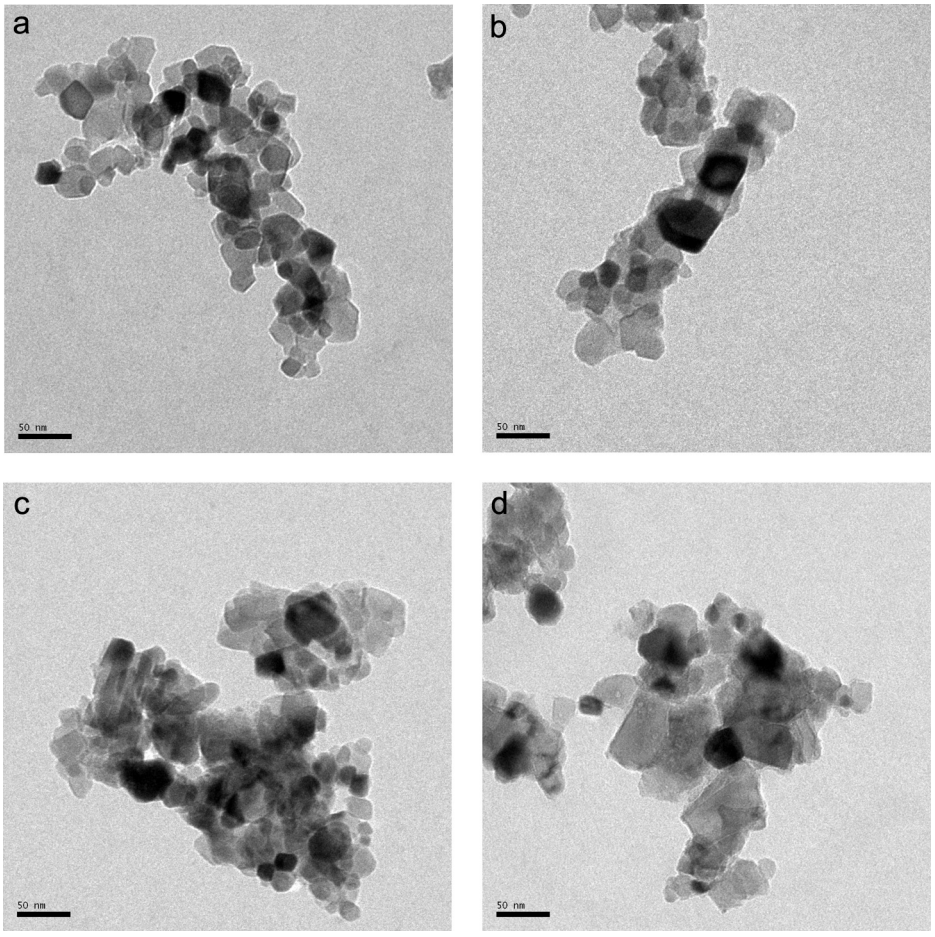


**Fig. 4.** TEM patterns of (a) 0.1$CuO/TiO_2$; (b) 0.1$NiO/TiO_2$; (c) 0.1$Co_3O_4/TiO_2$ and (d) 0.1$Fe_2O_3/TiO_2$.

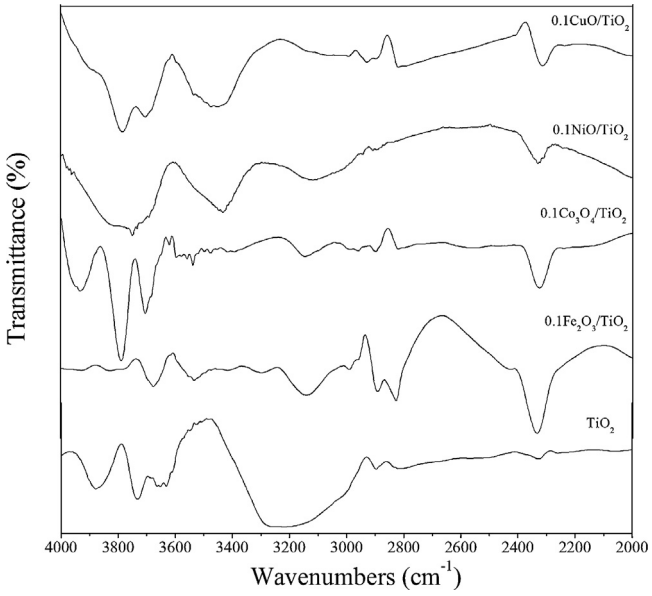


**Fig. 5.** FTIR spectra of $TiO_2$ and transition metal oxide loaded $TiO_2$.

irregular sizes and shapes. The distribution of particle size seems to be wider than those of other samples.

### 3.1.5. FT-IR spectroscopy

Hydroxyl radicals (•OH) have been deemed to be the major active species during the photocatalytic oxidation reaction. Hydroxyl radicals (•OH) produced during photocatalysis are suggested to be detected by FTIR spectroscopy, photoluminescence (PL) technique [26], and some test methods [27–29].

In our study, photocatalyst samples were analyzed by FTIR spectroscopy. FTIR spectra of samples showed O—H functional group and the bands at 3350 $cm^{-1}$ and 1620 $cm^{-1}$ represent the surface-adsorbed water and hydroxyl group [30]. Pure $TiO_2$ did not show any peaks at around 3350 $cm^{-1}$ and 1620 $cm^{-1}$ corresponding to the OH group in the FTIR spectra (Fig. 5). No peaks, therefore, corresponding to the OH group appears in FTIR spectra. On the other hand, for 0.1 wt% CuO on the $TiO_2$ catalyst, peaks appearing at 3427 and 1630 were observed. The concentration of the hydroxyl groups were measured as the integrated areas of corresponding peaks. Furthermore, the peaks identified at 3350 and 1620 $cm^{-1}$ correspond to the stretching and bending modes of molecularly adsorbed water [31]. When transition metals loaded, the shift to the higher wavenumbers were observed. However, the peak of iron is not significant.

The low energy interval the Ti—O bond bands are found at 1064 $cm^{-1}$ and below 1000 $cm^{-1}$. The peaks at 1112 $cm^{-1}$ suggest the presence of Ti—O—C bonds [32,33]. The band shifts with the addition of transition metal and changes between 1112 and 1116 $cm^{-1}$. The broad intense band below 1200 $cm^{-1}$ is due to Ti—O—Ti vibrations. Furthermore, the peak 1395 $cm^{-1}$ has been identified to be due to asymmetric bending vibrations of C—H bonds [34] and it changes between 1387 and 1402 $cm^{-1}$ with the addition of transition metals. A peak at 2327 $cm^{-1}$ is due to $CO_2$ adsorbed on the titania surface.

The as-prepared $CuO/TiO_2$ showed Cu—O absorptions around at 495 $cm^{-1}$ [35]. When CuO loaded with different content, the bands shifted between 492 and 500 $cm^{-1}$. Mainly two components, at 1049 $cm^{-1}$ and at 1125 $cm^{-1}$ are detected on $CuO/TiO_2$ in the C—O stretching region. The band at 546 $cm^{-1}$ is due to stretching vibrations Ti—O and Cu—O. In addition, the broad bands between 800 and 1400 $cm^{-1}$ are attributed to the lattice vibrations of titanium dioxide. The concentration of the hydroxyl groups first increases with the increase of Cu content and then decreases. However, the peak area was decreased after 0.1 wt% CuO loading. These results are in good agreement with activity results. This result indicated that the higher catalytic activity of $0.1CuO–TiO_2$ was attributed to a higher concentration of the hydroxyl groups of $0.1CuO–TiO_2$.

### 3.1.6. X-ray photoelectron spectroscopy

In order to confirm the chemical states of Fe, Co, Ni and Cu loaded on the $TiO_2$ samples, the experiments also do the XPS analysis. The results of XPS studies are shown in Fig. 6(a)–(d). As shown in Fig. 6a, the Fe 2p XPS peak is present at 711.1 eV. The high-resolution XPS spectrum of Co-loaded $TiO_2$ sample reveals the Co $2p_{3/2}$ and Co $2p_{1/2}$ peaks at 780.9 and 796.9 eV, respectively, as shown in Fig. 6b. Fig. 6c shows the Ni(2p) high-resolution XPS spectrum at the surface of a $Ni–TiO_2$ catalyst. It can be noted that the binding energies of Ni(2p3/2) and (2p1/2) were at 853.9 and 872.5 eV, respectively. It can be inferred that the element nickel was in the phase of NiO. Additionally, the XPS peak of Cu 2p at 935.8 eV is shown in Fig. 6d. So according to some literatures [36,37] and XPS analysis, it can be deduced that the Fe, Co, Ni and Cu loaded in photocatalysts are present as $Fe_2O_3$, $Co_3O_4$, NiO and CuO in the samples, respectively.

The Ti (2p1/2), Ti (2p3/2) binding energies were observed at 457.6 and 463.3 eV confirming the presence of $Ti^{4+}$. The binding energy at 528.7 eV is attributed to $O^{2-}$ ions of TiO2 frame work (Ti—O—Ti) [38–40].

The XPS analysis was carried out to identify the oxidation state of copper in the nanostructured $Cu–TiO_2$ samples. The survey and amplification of the selected spectra are respectively shown in Fig. 7. In Fig. 7, the characteristic peaks for the C 1s, Ti 2p, O 1s and Ti 2s core level binding energy (BE) in the 200–600 eV region can be seen. The C 1s peak (284.5 eV) corresponds to carbon, which is always present on the surface of the powdered samples (adventitious carbon). On the other hand, in the 960–920 eV binding energy region, the peak for the Cu 2p core level (BE) can be seen, whose intensity increases with the Cu content (samples with 0.05, 0.1 and 0.5 Cu wt%). Unfortunately, for the samples with 0.05, and 0.1 Cu wt%, the XPS equipment does not detect the Cu 2p spectrum, which is most probably due to the low content of copper in the sample. In Fig. 7, the deconvolution of the Cu 2p signal for the selected samples was resolved in Cu $2p^{1/2}$ and Cu $2p^{3/2}$ core level peaks, identifying the $Cu^0$ and $Cu^{1+}$ copper species. The presence of copper in the $Cu^{2+}$ oxidation state can be excluded because of the absence of the characteristic shake-up satellite lines of CuO, which are attributed to shake-up transitions by a ligand–metal 3d charge transfer that does not occur with Cu0 and $Cu^{+1}$ species, which have completely filled 3d shells [41].

## 3.2. Evaluation of photocatalytic activity

In general, the diffusion rate of adsorbed reactive species on the surface is faster than the photocatalytic reaction rate. Therefore, the photocatalytic reaction is the rate control step. The photocatalytic degradation can be described with the Langmuir–Hinshelwood equation [42]:

$$\frac{1}{r_0} = \frac{1}{k_r K_{ads} c_0} + \frac{1}{k_r}$$

$r_0$ is the initial reaction rate (mg $L^{-1}$ $min^{-1}$), $k_r$ the Langmuir–Hinshelwood reaction rate constant (mg $L^{-1}$ $min^{-1}$) and $K$ the Langmuir adsorption constant (L $mg^{-1}$).

The catalytic activities of all the synthesized Fe, Co, Ni and Cu loaded titania catalysts were evaluated toward the degradation of phenol under the optimized conditions and the results are shown in Fig. 8a and Table 1.

Fig. 8b presents the TOC removal results on the photocatalytic degradation of phenol with $0.1CuO/TiO_2$, $0.1NiO/TiO_2$,

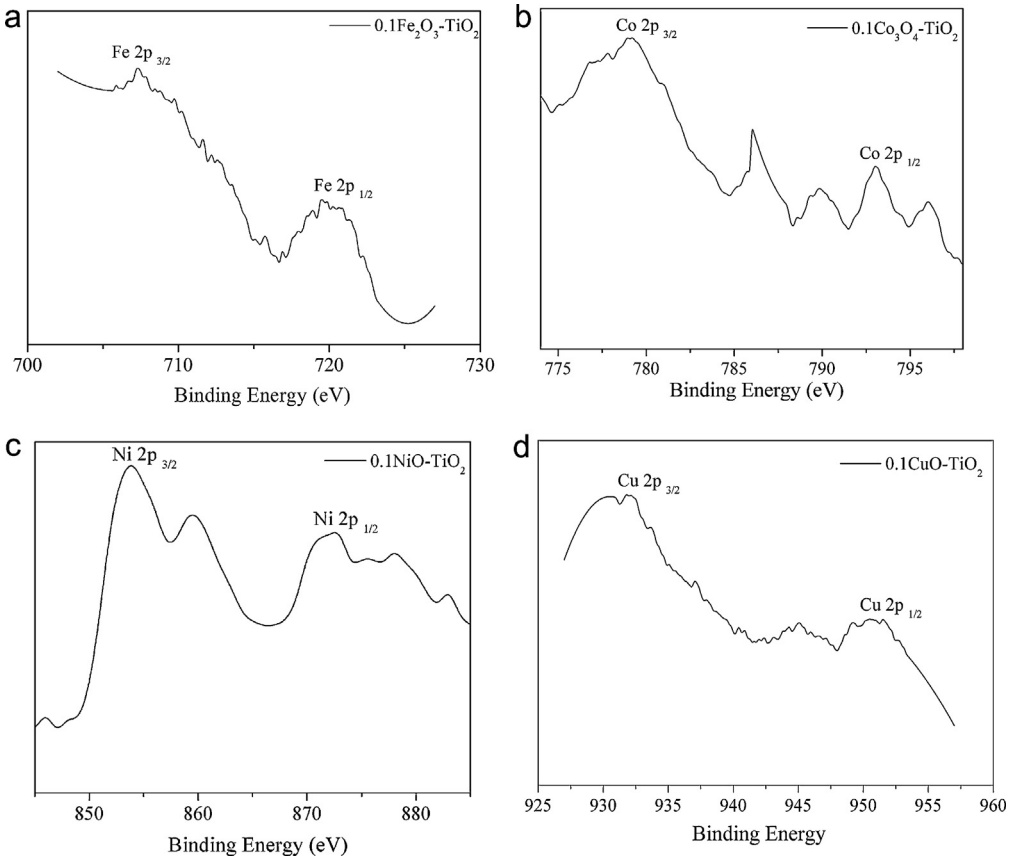


**Fig. 6.** (a) XPS spectra of Fe (2p) for $0.1Fe_2O_3/TiO_2$ catalyst. (b) XPS spectra of Co (2p) for $0.1Co_3O_4/TiO_2$ catalyst. (c) XPS spectra of Ni(2p) for $0.1NiO/TiO_2$ catalyst. (d) XPS spectra of Cu(2p) for $0.1CuO/TiO_2$ catalyst.

$0.1Co_3O_4/TiO_2$ and $Fe_2O_3/TiO_2$. 25 ppm phenol can be completely degraded in 90 min by $0.1CuO/TiO_2$ sample at an initial pH of 5 and 94% TOC removal can be achieved in 90 min This result emphasizes the achievement of the total mineralization. However, the TOC removal reached to 85% with the Degussa P25, which can completely degraded in 90 min.

$0.1CuO/TiO_2$ catalysts showed higher activity under UV irradiation than bare titania. Amongst nickel, cobalt and iron titania catalysts, $0.1NiO/TiO_2$ catalyst showed higher photocatalytic activity than $0.1Co_3O_4/TiO_2$ and $Fe_2O_3/TiO_2$ catalysts.

The performance of $CuO/TiO_2$ catalysts with varying CuO loadings was also studied (Fig. 9). The degradation ability for the $CuO/TiO_2$ catalyst increased with an increase in the amount of CuO loadings to $TiO_2$. The 0.1 wt% CuO showed the highest percentage of phenol degradation (100%), however, after that weight percentage, the photocatalytic activity decreased slightly with further loadings of $TiO_2$ (Table 1). In addition, phenol degradation decreases from

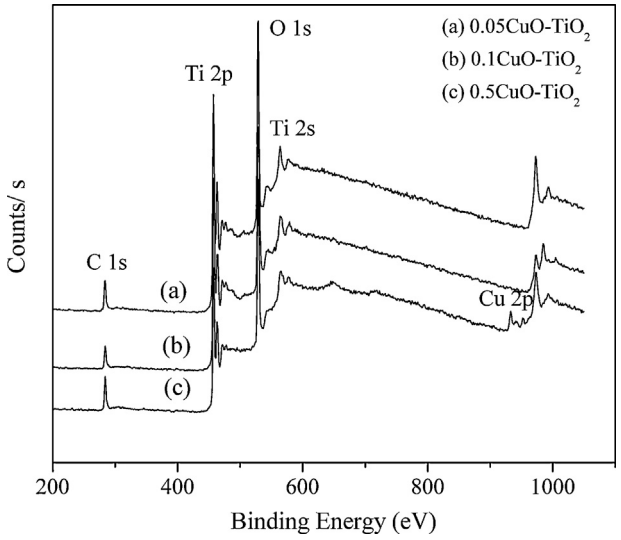


**Fig. 7.** XPS spectra of C 1s, Ti 2p, Ti 2s and O 1s for $CuO–TiO_2$ samples.

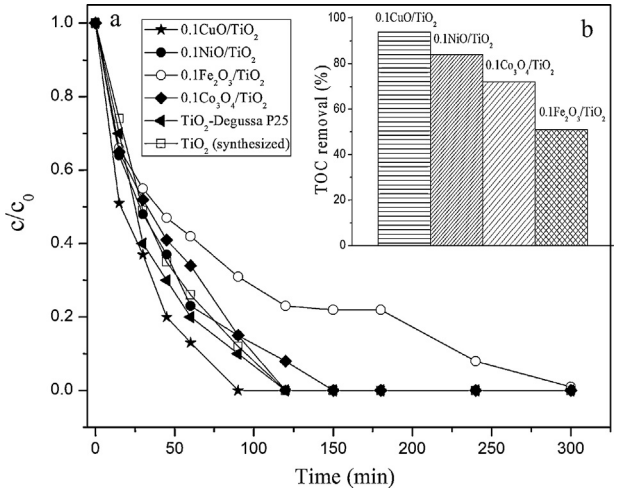


**Fig. 8.** (a) Time course of the adsorption of phenol by $TiO_2$ (synthesized), $TiO_2$ (P25) and transition metal oxide loaded $TiO_2$ under UV irradiation. (b) Inset shows the impact of transition metal oxide on TOC removal in the phenol degradation.

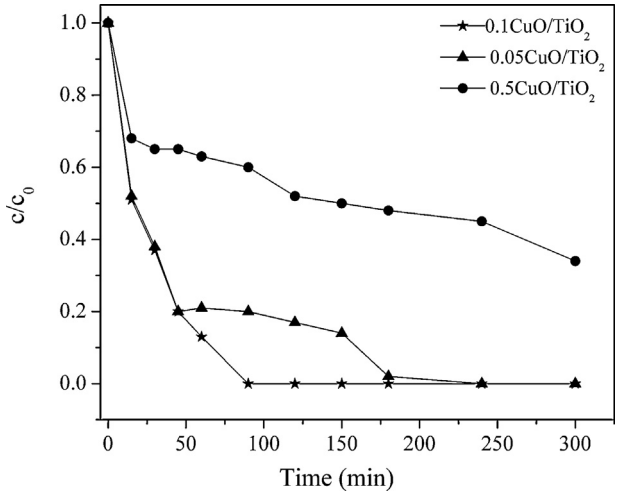


**Fig. 9.** Effect of various CuO loading on phenol photodegradation at 25 °C.

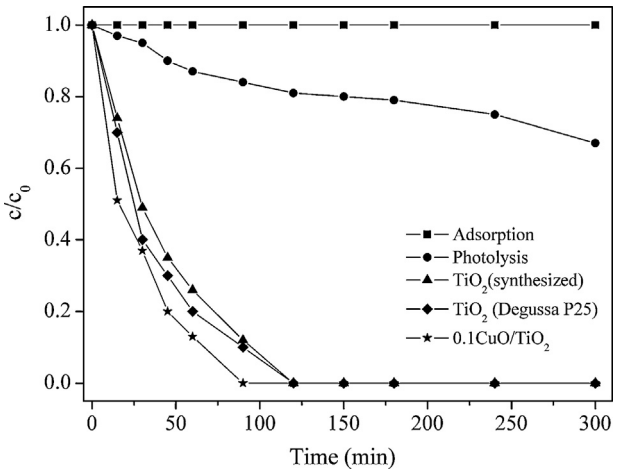


**Fig. 10.** Time course of the adsorption of phenol by 0.1CuO/$TiO_2$ in dark, the photolysis of phenol, and the degradation of phenol by 0.1CuO/$TiO_2$ under UV irradiation.

100 to 40% with the 0.5 wt% CuO mixed with $TiO_2$. In fact, a decrease in activity could probably be explained by partial blocking of the active species of $TiO_2$ due to the formation of larger CuO particles at higher CuO loadings. The results showed that surface area and particle size of samples were changed with the loading of CuO. Addition to this result, tendency of CuO to form larger particles on $TiO_2$ surface has also caused to lower the conversion of phenol.

Yu and Ran investigated photocatalytic behavior of $Cu(OH)_2$ clusters-modified $TiO_2$ (P25 Degussa) for hydrogen production. The deposition of $Cu(OH)_2$ clusters on the surface of $TiO_2$ was achieved different mol% ratio (0, 0.05, 0.25, 1, 2, and 7) by a facile precipitation method. The highest $H_2$-production rate was obtained with 0.29 mol $Cu(OH)_2$ loading content. This was ascribed to the fact that small $Cu(OH)_2$ clusters was uniformly dispersed on the surface of the $TiO_2$ nanoparticles [43].

Among the transition metal oxide loaded-$TiO_2$ catalysts, $Fe_2O_3/TiO_2$ showed maximum of 68% degradation of phenol within 90 min and complete decomposition at 300 min. Hence, comparison of degradation efficiencies of all other catalysts under UV irradiation at 90 min has been made.

Xu and Yu prepared Fe-modified $TiO_2$ nanotube arrays ($TiO_2$ NTs) and investigated photoelectrocatalytic (PEC) degradation of methylene orange (MO) and 4-chlorophenol in water under visible-light irradiation ($\lambda > 420$ nm) [44]. The results showed that a Fe-modified $TiO_2$ NTs electrode exhibited a larger photocurrent response and higher photoelectrocatalytic activity for the degradation of organic pollutants than a pure $TiO_2$ NTs electrode. A higher photocurrent response is due to more photogenerated electron–hole pairs produced, a lower electron–hole recombination rate and higher photoelectron-transfer efficiency. A higher photocurrent response also implies the Fe-modified $TiO_2$ NTs electrode has a higher PEC activity [44].

In our study, the catalytic activity of 0.1 wt% CuO to $TiO_2$ was found to be higher than nano $TiO_2$ prepared and P-25. Moreover, there was a similar pronounced relationship between in surface area and catalytic activity (Table 1). The highest in surface area and activity was for 0.1CuO/$TiO_2$ catalyst.

Similiarly, Yu et al, reported the fabrication of CuO–$TiO_2$ composite photocatalysts by impregnation of commercial P25 titania with copper nitrate [45]. The study of CuO effect on the photocatalytic $H_2$-production rates showed that CuO clusters could act as an effective co-catalyst enhancing photocatalytic activity of $TiO_2$. The fluorescence quenching experiments further confirm the transfer of photogenerated electrons from $TiO_2$ to CuO clusters and the favorable contact between CuO clusters and $TiO_2$ nanoparticles [46–48].

The adsorption (dark experiment), photolysis (experiment under illumination and no catalyst) and photodegradation (experiment under illumination) of phenol on 0.1CuO/$TiO_2$ are shown in Fig. 10. It can be clearly seen that the adsorption of phenol on the surface of 0.1CuO/$TiO_2$ material is negligible. The photolysis of phenol under the UV irradiation is about 19% in 2 h. 0.1CuO/$TiO_2$ sample exhibits a much higher efficiency in degradation of phenol than pure $TiO_2$ and Degussa-P25.

Xu et al., investigated the photocatalytic activity of titanium oxide supported on ZSM5, zeolite A, silica, and alumina using the photooxidation of 4-chlorophenol and acetophenone. It was found that the photocatalytic activity of $TiO_2$/ZSM5 was higher than $TiO_2$ powder prepared and Degussa P25 [49].

Wu et al., have described the formation of a mutual chemical interaction between the pure oxides when they are coprecipitated together, leading to a profound effect on the photocatalytic properties [50].

The catalyst prepared with impregnation method showed the low activity. The conversion of phenol has reached to 68% at the end of the 90 min by using the 0.1CuO/$TiO_2$. This result may show that bulk CuO may not improve the photodegradation. Agglomeration is seen in the SEM photograph of catalyst prepared by impregnation method. The morphology of the catalyst prepared by SSD method is different from impregnation. The primary particles exhibit irregular sizes and shapes. The distribution of particle size seems to be wider than those of other sample. Based on the TEM photograph of catalyst, CuO cluster is more effective in photodegradation reactions.

Yu et al., reported the photocatalytic activity of CuO clusters and bulk CuO for $H_2$-production. The conduction band edge of $TiO_2$ is higher than that of CuO clusters and bulk CuO [45]. The conduction band edge of bulk CuO has a less negative potential than $H^+/H_2$ potential. On the contrary, the conduction band edges of CuO clusters are deemed to be higher than that of bulk CuO due to the quantum confinement effect and more negative than $H^+/H_2$ potential [51]. Photogenerated electrons transfer from the conduction band of $TiO_2$ into CuO clusters and bulk CuO, and accumulate at their lower conduction bands, while holes accumulate at the valence band of $TiO_2$ and CuO. Consequently, the photogenerated electron in CuO clusters can effectively reduce $H^+$ to produce $H_2$. Although bulk CuO is activated by the UV-LED light, also photogenerated electrons can be transferred from the conduction band of $TiO_2$ into that of bulk CuO, which resulted in a low activity of the sample CT9.0 [45].

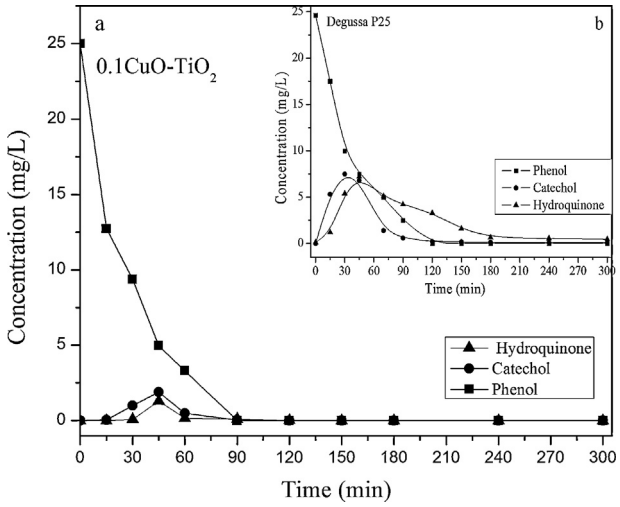


**Fig. 11.** Concentration profiles for phenol, catechol and hydroquinone obtained during the photocatalytic oxidation reaction using (a) $0.1CuO/TiO_2$ and (b) Degussa P25.

The activity of the photocatalyst is influenced by its crystallinity as well as other factors such as surface area, crystal size, synthesis method, band gap, crystal phase and surface OH group.

The results of HPLC studies of photocatalytic reaction show phenol concentration decays following a pseudo first order rate law, reaching at the end of the photocatalytic run essentially zero concentration and the concentration of the main reaction intermediates initially rise and then decrease until almost complete disappearance at the same time of complete phenol conversion.

HPLC analysis performed during the photocatalytic degradation of phenol. Hydroquinone (HQ; 4-hydroxyphenol) and Catechol (CT; 2-hydroxyphenol) were detected as intermediates. And also ring-opening products are supposed to be short chain acids, such as, acetic acid, maleic acid, oxalic acid, etc. [52], they were identified by GC–MS analysis.

Concentration profiles for phenol, catechol and hydroquinone obtained during the photocatalytic oxidation reaction using $0.1CuO/TiO_2$ are shown in Fig. 11a. Besides, the distributions of intermediates also were compared in different binary oxide catalysts. According to HPLC results, two intermediates, HQ and CT, were detected in very low concentration during the degradation of phenol for metal oxide loaded-$TiO_2$ catalysts.

It is noteworthy to mention that, ring-opening products were detected in higher concentration by using metal oxide loaded-$TiO_2$ catalysts compared to Degussa P-25 (Fig. 11b). These intermediates undergo further photocatalytic oxidation to ring cleavage to yield carboxylic acids and aldehydes, which give $CO_2$ and $H_2O$ due to decarboxylation.

Fig. 10b shows the phenol decomposition on Degussa P-25. It can be seen that hydroquinone and catechol for the Degussa P-25 were found in higher concentration compared to $0.1CuO/TiO_2$. It should be noted that, some structural features of catalyst play a significant role during the photocatalysis.

These results may also indicate that the photochemical reaction plays an important role for the degradation of phenol under these conditions.

## 4. Conclusions

Copper, nickel, cobalt and iron oxide loaded titania catalysts were synthesized successfully by simple solid-state method. TEM and XPS measurements also confirmed the existence of metal oxides over titania semiconductor surface. According to TEM-EDS analysis, NiO, $Co_3O_4$ and $Fe_2O_3$ showed lower dispersion on nano $TiO_2$ than CuO. The enhanced adsorption of phenol over the catalyst surface and decrease in particle size as a result of $Cu^{2+}$ loading is suggested to be the cause for higher activity of the catalyst.

$0.1CuO/TiO_2$ catalyst was found to be better photocatalyst than bare TiO2 toward the degradation of phenol. The transfer of electrons from CuO to $TiO_2$ was seen to the main phenomena in the binary oxide catalyst through chemical interactions between CuO and $TiO_2$ in the form of the Ti—O—Cu— bond.

The 0.1CuO wt% $TiO_2$ showed the highest percentage of phenol degradation (100%) and highest reaction rate ($0.99\ mg\ l^{-1}\ min^{-1}$) in 90 min. In addition, the catalytic activity of $0.1CuO/TiO_2$ was found to be higher than nano $TiO_2$ and P-25 photocatalyst.

The catalytic activity was affected by the preparation method. Comparatively, the phenol degradation over $0.1CuO/TiO_2$(IMP) after 90 min was 68%.

## Acknowledgement

This work was supported by the Research Fund of the Istanbul University.

## References

[1] L.H. Keith, W.A. Telliard, Environmental Science and Technology 13 (1979) 416–423.
[2] V.M. Brown, D.H.M. Jordan, B.A. Tiller, Water Research 1 (1967) 587–597.
[3] J.W. Pattersom, Wastewater Treatment Technology, Ann Arbor Science Pub, Inc., Ann Arbor, MI, 1985, pp. 199–215.
[4] R.L. Autenrieth, J.S. Bonner, A. Akgerman, E.M. McCreary, Journal of Hazardous Materials 28 (1991) 29–53.
[5] C. Hu, Y.Z. Wang, H.X. Tang, Chemosphere 41 (2000) 1205–1209.
[6] G. Colon, J.M. Sanchez-Espana, M.C. Hidalgo, J.A. Navio, Journal of Photochemistry and Photobiology A: Chemistry 179 (2006) 20–27.
[7] M.A. Barakat, H. Schaeffer, G. Hayes, S. Ismat-Shah, Applied Catalysis B: Environmental 57 (2005) 23–30.
[8] A. Fujishima, T.N. Rao, D.A. Tryk, Journal of Photochemistry and Photobiology C: Photochemistry Reviews 1 (2000) 1–21.
[9] I. Salem, Catalysis Reviews 45 (2003) 205–296.
[10] D. Fabbri, A.B. Prevot, E. Pramauro, Applied Catalysis B: Environmental 62 (2006) 21–27.
[11] R. Asahi, T. Morikawa, T. Ohwaki, K. Aoki, Y. Taga, Science 293 (2001) 269–271.
[12] G. Lu Jr., J.T. Yates, Chemical Reviews 95 (1995) 735–758.
[13] S. Kim, S. Hwang, W. Choi, Journal of Physical Chemistry B 109 (2005) 24260–24267.
[14] T.J. Kemp, R.A. McIntyre, Polymer Degradation and Stability 91 (2006) 165–194.
[15] I. Tseng, J.C.S. Wu, H. Chou, Journal of Catalysis 221 (2004) 432–440.
[16] J. Zhu, W. Zheng, B. He, J. Zhang, M. Anpo, Journal of Molecular Catalysis A: Chemical 216 (2004) 35–43.
[17] H.Q. An, J.X. Li, J. Zhou, Journal of Materials Chemistry 20 (2010) 603–610.
[18] M.A. Khan, S.I. Woo, O.B. Yang, International Journal of Hydrogen Energy 33 (2008) 5345–5351.
[19] M. Zhou, J. Yu, B. Cheng, Journal of Hazardous Materials B137 (2006) 1838–1847.
[20] R. Janes, L.J. Knightley, C.J. Harding, Dyes and Pigments 62 (2004) 199–212.
[21] T.Y. Han, C.F. Wu, C.T. Hsieh, Journal of Vacuum Science and Technology B 25 (2007) 430–435.
[22] M.S. Nahar, K. Hasegawa, S. Kagaya, S. Kuroda, Science and Technology of Advanced Materials 8 (2007) 286–291.
[23] A. Kambur, G.S. Pozan, I. Boz, Applied Catalysis B: Environmental 115/116 (2012) 149–158.
[24] S. Rengaraj, X.Z. Li, Journal of Molecular Catalysis A: Chemical 243 (2006) 60–67.
[25] Z. He, L. Xie, S. Song, C. Wang, J. Tu, F. Hong, Q. Liu, J. Chen, X. Xu, Journal of Molecular Catalysis A: Chemical 319 (2010) 78–84.
[26] Q. Xiang, J. Yu, P.K. Wong, Journal of Colloid and Interface Science 357 (2011) 163–167.
[27] Q. Xiang, J. Yu, W. Wang, M. Jaroniec, Chemical Communications 47 (2011) 6906–6908.
[28] K. Ishibashi, A. Fujishima, T. Watanabe, K. Hashimoto, Electrochemistry Communications 2 (2000) 207–210.
[29] J.G. Yu, W.G. Wang, B. Cheng, B.L. Su, Journal of Physical Chemistry C 113 (2009) 6743–6750.
[30] L. Wu, J.C. Yu, L. Zhang, X. Wang, W. Ho, Journal of Solid State Chemistry 177 (2004) 2584–2590.
[31] S. Sakthivel, M.C. Hidalgo, D.W. Bahnemann, S.U. Geissen, V. Murugesan, A. Vogelpohl, Applied Catalysis B: Environmental 63 (2006) 31–40.
[32] T. Ivanova, A. Harizanova, Surtchev, Materials Letters 55 (2002) 327–333.

[33] M.T. Harris, A. Singhal, J.L. Look, J.R. Smith-Kristensen, J.S. Lin, L.M. Toth, Journal of Sol–Gel Science and Technology 8 (1997) 41–47.
[34] T. Lo'pez, J.A. Moreno, R. Go'mez, X. Bokhimi, J.A. Wang, H. Yee-Madeira, G. Pecchi, P. Reyes, Journal of Materials Chemistry 12 (2002) 714–718.
[35] J.X. Xia, H.M. Li, Z.J. Luo, H. Shi, K. Wang, H.M. Shu, Y.S. Yan, Journal of Physics and Chemistry of Solids 70 (2009) 1461–1464.
[36] M.C. Long, W.M. Cai, J. Cai, B.X. Zhou, X.Y. Chai, Y.H. Wu, Journal of Physical Chemistry B 110 (2006) 20211–20216.
[37] A. Hameed, M.A. Gondal, Z.H. Yamani, Catalysis Communications 5 (2004) 715–719.
[38] Y.V. Zubavichus, Y.L. Slovokhotov, M.K. Nazeeruddin, S.M. Zakeeruddin, M. Gratzel, V. Shklover, Chemistry of Materials 14 (2002) 3556–3563.
[39] C. Elmasides, D.I. Kondarides, W. Grunert, X.E. Verykios, Journal of Physical Chemistry B 103 (1999) 5227–5239.
[40] H.H. Tseng, M.C. Wei, S.F. Hsiung, C.W. Chioua, Chemical Engineering Journal 150 (2009) 160–167.
[41] C.D. Wagner, W.M. Riggs, L.E. Davis, J.F. Moulder, G.E. Mullenberg, Handbook of X-ray Photoelectron Spectroscopy, Perkin-Elmer Corp., Eden Prairie, MN, USA, 1979.
[42] Y. Xu, C.H. Langford, Journal of Photochemistry and Photobiology A 133 (2000) 67–71.
[43] J. Yu, J. Ran, Energy and Environmental Science 4 (2011) 1364–1371.
[44] Z. Xu, J. Yu, Nanoscale 3 (2011) 3138–3144.
[45] J. Yu, Y. Hai, M. Jaroniec, Journal of Colloid and Interface Science 357 (2011) 223–228.
[46] J.G. Yu, L.F. Qi, M. Jaroniec, Journal of Physical Chemistry C 114 (2010) 13118–13125.
[47] J.G. Yu, J.F. Xiong, B. Cheng, S.W. Liu, Applied Catalysis B: Environmental 60 (2005) 211–221.
[48] B. Cheng, Y. Le, J.G. Yu, Journal of Hazardous Materials 177 (2010) 971–977.
[49] Y. Xu, C.H. Langford, Journal of Physical Chemistry 99 (1995) 11501–11507.
[50] J.-C. Wu, C.-S. Chung, C.-L. Ay, I. Wang, Journal of Catalysis 87 (1984) 98–107.
[51] W.K. Ho, J.C. Yu, J. Lin, J.G. Yu, P. Li, Langmuir 20 (2004) 5865–5869.
[52] B. Tryba, A.W. Morawski, M. Inagaki, M. Toyoda, Applied Catalysis B: Environmental 63 (2006) 215–221.